Integrated geophysical survey of an earthen dam using electrical resistivity tomography and UAV-derived topographic data

Balgaisha Mukanova[1*], Kambar Assemov[2], Yermek Akhmetov[2], Alibek Taskynbayev[2]

[1]*Department of Computational and Data Science, Astana IT University, Astana, Kazakhstan.*
[2]*National Center for Complex Processing of Mineral Raw Materials of the Republic of Kazakhstan, Almaty, Kazakhstan.*

Corresponding author: Balgaisha Mukanova (*Email: balgaisha.mukanova@astanait.edu.kz*)

Abstract

This study aims to improve the detection of internal seepage zones in earthen dams by integrating Electrical Resistivity Tomography (ERT), UAV-derived topographic data, and GIS technology. Monitoring the internal condition of hydraulic structures is essential to identify potential failure risks before they become critical. The methodology involved acquiring ERT profiles along multiple profiles along a dam, with electrode elevations first measured using GPS and then corrected using high-resolution digital elevation models (DEMs) generated from UAV surveys. These datasets were processed and analyzed within a GIS environment to assess the impact of elevation accuracy on subsurface modeling. The findings revealed that the inclusion of UAV-based DEMs improved the vertical resolution of geoelectrical models, reducing depth estimation errors and allowing for more precise delineation of subsurface anomalies. Four low resistance zones ($<20\ \Omega \cdot m$) were detected at depths of 15–25 meters, spatially aligned with visible signs of seepage and erosion. The results demonstrate that combining geophysical surveys with remote sensing based on UAVs enhances the reliability of dam condition assessments. This integrated, non-invasive approach provides a cost-effective and scalable solution for routine dam safety monitoring and retrospective analysis, offering practical value for infrastructure managers, engineers, and regulatory agencies.

Keywords: Dam monitoring, Digital elevation model, Drone, ERT, GIS technology.

Competing Interests: The authors declare that they have no competing interests.
Authors' Contributions: All authors contributed equally to the conception and design of the study. All authors have read and agreed to the published version of the manuscript.
Transparency: The authors confirm that the manuscript is an honest, accurate, and transparent account of the study; that no vital features of the study have been omitted; and that any discrepancies from the study as planned have been explained. This study followed all ethical practices during writing.

1. Introduction

Earthen dams have historically played a vital role in water management for agricultural, domestic, and industrial purposes. Today, they account for approximately 67% of all registered dams globally [1] with some, such as the Rogun and Nurek dams in Tajikistan, reaching heights of over 300 meters. Despite their widespread use, many of these structures are aging and deteriorating, raising concerns about their structural integrity and long-term safety. Failures of earthen dams, particularly those under 70 meters in height and constructed during the second half of the 20th century, are projected to increase in frequency due to material fatigue, poor maintenance, and increased hydrostatic pressure. These failures often result in severe environmental, economic, and human losses. Furthermore, the intensification of climate change and the growing occurrence of extreme weather events, including floods and prolonged droughts, pose additional stress on dam infrastructure, emphasizing the urgent need for improved monitoring and assessment strategies [2].

Traditional monitoring techniques, such as visual inspections and borehole investigations, are often limited in their ability to detect early-stage internal defects. In this context, non-invasive geophysical methods have emerged as valuable tools for evaluating the subsurface conditions of hydraulic structures. Among them, Electrical Resistivity Tomography (ERT) has gained considerable attention due to its cost-effectiveness, operational simplicity, and ability to detect anomalies associated with internal erosion, seepage, and moisture variations [3]. ERT has proven effective in a range of geotechnical and hydrogeological applications, including slope stability analysis, groundwater monitoring, and permafrost investigations [4, 5]. Despite its advantages, ERT measurements are highly sensitive to the accuracy of topographic data, particularly in heterogeneous terrains, which can limit the resolution and reliability of the interpreted results.

To address this limitation, this study proposes an integrated approach that combines ERT with high-resolution digital elevation models (DEMs) obtained from unmanned aerial vehicles (UAVs). UAV-based photogrammetry offers a rapid and non-contact method for capturing detailed surface topography, which can significantly enhance the quality of geoelectrical models by providing precise electrode elevations and improved spatial referencing.

The main objectives of this research are: (i) to evaluate the effectiveness of combining ERT and UAV-derived DEMs for detecting seepage zones in an earthen dam, (ii) to quantify the impact of topographic accuracy on the quality of resistivity models, and (iii) to demonstrate the potential of this integrated method for the evaluation of operational dam safety. The research questions guiding this study are as follows:

- How does the inclusion of UAV-derived elevation data affect the accuracy of ERT-based subsurface imaging?
- Can this integrated method reliably identify internal seepage zones that correlate with visible surface anomalies?

To answer these questions, the study was conducted in an earthen dam in southern Kazakhstan using a series of geophysical profiles and UAV-based surveys.

The paper is organized as follows: Section 2 presents a review of the literature, Section 3 describes the study site and outlines the research methodology, Section 4 is devoted to the discussion of the results, and Section 5 presents the conclusion.

2. Literature Review

Electrical Resistivity Tomography (ERT) has proven particularly effective in diagnosing reservoir embankment dams, as it enables the rapid detection of water-saturated zones within the dam body. The use of modern multichannel equipment facilitates the acquisition and processing of large volumes of data, contributing to the generation of more accurate geoelectrical cross-sections. Numerous studies have confirmed the efficacy of ERT in assessing the condition and geotechnical properties of soils within earthen dam structures [6-9].

However, the interpretation of ERT data is known to be sensitive to measurement inaccuracies and surface heterogeneities of the investigated medium [10, 11]. As such, incorporating data from additional sources can enhance both the reliability and accuracy of ERT-based assessments. In most cases, these supplementary data are provided by other geophysical methods, enabling a multi-method integration approach tailored to specific investigative goals.

For example, a suite of geophysical techniques, including ERT, controlled-source audio-frequency magnetotellurics (CSAMT), gravity surveys, and seismic refraction, was used alongside geological mapping during the construction of the Neutrino Laboratory in China [12]. Similarly, the study in Isaev et al. [13] demonstrated that the combination of multiple geophysical methods improves inverse modeling and refines subsurface characterization. That study also incorporated artificial intelligence (AI) tools for interpretation, complementing traditional analytical techniques.

In another case Sentenac et al. [14] the sequential application of electromagnetic sounding, ERT, and the self-potential (SP) method effectively identified potential seepage pathways in an earthen dam, highlighting the benefits of integrated methodologies. The significance of such combined geophysical approaches, particularly under low signal-to-noise conditions and operational constraints, is emphasized in urban geological mapping research [15]. Moreover, the integration of geophysical data into reservoir modeling workflows for improved subsurface interpretation is discussed in Azevedo and Soares [16].

The rapid development of unmanned technologies has enabled their use for various purposes. Thus, UAVs have been used for environmental monitoring of air quality in the industrial and urbanized regions of Kazakhstan. The effectiveness of UAVs for structural diagnostics of hard-to-reach elements of a century-old metal arch bridge in Spain is demonstrated. This has led to increased accuracy in the structural inspection of the bridge, reduced costs, and minimized hazards for workers. An interesting experience of using drones for autonomous unmanned pollination of gardens in Oman is summarized. The article discusses the advantages and disadvantages of this method and analyzes its effects on yield, fruit quality, etc.

In recent years, the combination of remote sensing with ground-based geophysical surveys has gained increasing traction. For example, drone imagery is often integrated with ERT to classify land cover types and surface characteristics [17, 18]. The authors of Junaid et al. [19] proposed a rapid slope stability assessment technique that combines UAV photogrammetry and 2D ERT. UAV-derived 3D point clouds were used to extract discontinuity orientations, while ERT revealed fracture persistence within the subsurface. Their results confirmed the method's capability to quantify slope failure risks, including planar and flexural toppling. In the context of quarry design, a virtual 3D model of a marble deposit is developed by integrating UAV-based surface photogrammetry with subsurface images of Vertical Electrical Sounding (VES) Hussain et al. [20]. Data was processed using open-source 3D modeling tools, resulting in optimized quarry layouts and safer extraction zones.

The soil moisture dynamics in a historical earth-filled dam in the Czech Republic were monitored using a hybrid approach that combined ERT, close-range photogrammetry, and UAV-based thermal imaging [21]. This allowed for the detection of water seepage, internal erosion, and material heterogeneity. The authors of Antoine et al. [22] have combined ERT, Ground Penetrating Radar (GPR), and UAV-based terrain modeling to assess the internal structure and integrity of a test dike within the European project Polder2C. Their integrated 3D application improved the interpretation of the data for future experimental campaigns.

The use of drone geophysical data has helped improve the efficiency of archaeological investigations in various geological conditions [23, 24]. The authors of Dadrass Javan et al. [25] who cited more than 435 publications, highlighted that rotary UAVs and imaging-based methods dominate current research. The review emphasizes the growing role of sensor integration and multi-source data fusion in UAV geophysics.

The use of UAVs in dam and levee surveys can be considered a valuable source of topographic data. UAVs provide rapid access to high-resolution imagery of the dam surface and surrounding terrain, as well as detailed digital surface models (DSMs). In Zhao et al. [26], UAV-derived data were used to correct coordinate inaccuracies in reservoir zones using the Structure-from-Motion (SfM) algorithm, while infrared imaging onboard supported seepage detection.

Long-term monitoring with high-resolution UAVs has been adopted in China to detect structural changes in dam infrastructure [17]. In Dong et al. [18] an automated method for crack detection based on high-resolution UAV imagery was proposed, demonstrating the potential of UAVs to monitor structural health.

This study explores the use of UAV-derived topographic data to enhance the accuracy of geophysical investigations of earthen dams using the ERT method. To the best of our knowledge, this specific approach to refining ERT interpretation through UAV integration is novel. The data obtained from ERT and UAV sources are intended for incorporation into a geoinformation system currently being developed by the authors for dam and levee monitoring in the Republic of Kazakhstan [27]. This system aims to consolidate diverse datasets, including geophysical surveys and aerial vehicle imagery, for a comprehensive assessment of dam safety.

3. Materials and Methods

In this study, an integrated approach combining Electrical Resistivity Tomography (ERT) and UAV-derived topographic data is used to assess the internal condition of an earthen dam. ERT was used to identify subsurface anomalies, such as seepage pathways, by measuring variations in electrical resistivity. High-resolution elevation data obtained via UAV-based photogrammetry enabled precise georeferencing of electrode positions. This combination improves spatial accuracy in resistivity modeling, which is particularly important for small to medium-sized dams.

Unlike conventional ERT studies that rely on GPS-based coordinate measurements, which typically exhibit vertical uncertainties of ±3–5 meters, our approach uses UAV-derived Digital Surface Models (DSMs) to correct for such inaccuracies. This reduces vertical error to within ±0.1 meters, enabling more reliable mapping of internal anomalies. To our knowledge, no previous studies in the region have directly integrated UAV-derived elevation data into the processing and interpretation of ERT survey results. This constitutes the key methodological novelty of the present work.

3.1. ERT Survey Conditions

The field survey was conducted in the spring of 2024 at the K-28 reservoir dam in the Karasai District of the Almaty Region, Kazakhstan. The dam was constructed in 1971 and primarily serves for agricultural irrigation. It has a total length of 340 meters and a height of 20 meters. A concrete tubular spillway, 128.5 meters long, is integrated into the dam body.

Geophysical investigations were conducted along the downstream slope of the dam. The preparation of the topographic data, including the marking and referencing of profiles and pickets, was carried out with a Garmin GPSMAP 65 navigator [28], which logged X and Y coordinates in the WGS 84 UTM coordinate system, taking into account the geoid surface. The coordinates of the start and end points of each profile were entered into the GPS device to assist in field orientation.

Ten geophysical profiles were laid out, each 235 meters long and spaced 5 meters apart. The distance between the pickets along each profile was also 5 meters. The profile length of 235 meters corresponds to the width of the reservoir in the upstream section. These profiles were positioned to cover the entire downstream slope of the dam. Figure 1 shows the ERT profile layout scheme.

Figure 1.
Scheme of the electrical resistivity tomography profiles.

The ERT technique measures the apparent electrical resistivity, which varies with the physical properties of the subsurface materials. This method involves injecting a direct current into the ground and measuring the resulting difference in electric potential at various electrode spacings.

During the survey, electrodes placed along each profile were alternately used as current injectors and potential receivers, increasing the measurement density compared to traditional vertical electrical sounding methods, which typically provide limited lateral resolution. A direct current was applied, and the voltage responses were recorded using multiple electrode configurations. The apparent resistivity values were subsequently calculated using modeling and inversion algorithms implemented in specialized software packages [29, 30]. Common array configurations for ERT such as Schlumberger, Wenner, dipole-dipole, and three-electrode arrays, can be used depending on the survey objectives [31]. The sequence in which electrodes function as current or potential electrodes is defined by the selected protocol (see Figure 2).
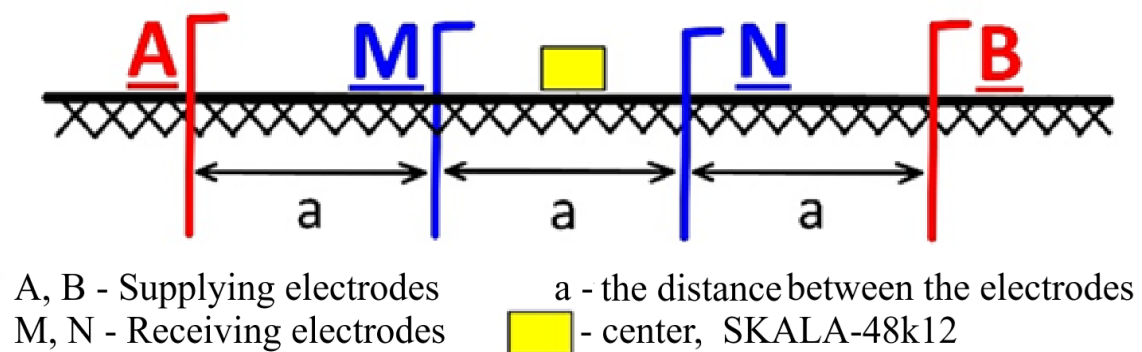

A, B - Supplying electrodes
M, N - Receiving electrodes
a - the distance between the electrodes
▢ - center, SKALA-48k12

Figure 2.
Schematic diagram of electrode installation.

Stainless steel rods (30 cm in length) were used as electrodes. Data acquisition was performed using the ERT system "SKALA-48K12" [32], which features an automatic switching module to activate electrode pairs according to the protocol defined by the operator. The electrodes were connected through multi-core cables with 5-m spacing.

Data were processed using the ZondRes2D software package [30], which performs direct and inverse modeling based on the finite element method (FEM), offering greater accuracy than traditional finite difference methods (FDM). As a result, two-dimensional resistivity sections were generated for all 10 profiles.

3.2. Coordinates Determination

The positioning error of the Garmin-65 GPS navigator was approximately ±3 meters in both horizontal and vertical directions. Inaccuracies in this device arise from the inherent limitations of signal reception within the GPS satellite navigation system and are within the expected accuracy range, with a nominal accuracy of ±3.65 meters [28].

To improve the spatial accuracy of the geophysical data, the elevations measured using the GPS device were compared to those obtained from a UAV survey. UAV surveys typically produce a Digital Surface Model (DSM), which includes the heights of all surface features such as buildings and vegetation. In this case, the area of interest lacks significant above-ground structures, so the DSM was assumed to approximate the Digital Elevation Model (DEM).

Aerial photogrammetry was conducted using a DJI Phantom 4 RTK drone for precise georeferencing of the geophysical profiles in both horizontal and vertical dimensions. This system provides horizontal and vertical positioning accuracy within ±0.1 meters [33]. The DJI Terra Overseas software was used to process UAV data, which produced high-resolution orthophotos and DSMs [34]. These outputs were integrated into a terrain map in ArcGIS 3.4.3 [35] onto which the electrode positions were plotted.

A comparison between GPS-derived elevations and those from the UAV-based DSM revealed an average elevation offset of 37–41 meters along the profiles. The survey site is located near 76.535° E and 43.285° N. In this area, the difference between the ellipsoidal and geoid heights is approximately 44.5 meters, as reported by the GeoidEval service [36].

Therefore, to convert UAV-derived elevations (in EPSG:4326 - WGS 84 ellipsoidal heights) to orthometric (geoid) heights, a correction factor of +44.5 meters is required. In this study, where relative elevation differences are more significant than absolute values, a constant correction value of +39.6 meters was chosen, representing the average observed offset, to synchronize UAV and GPS elevation data during interpretation.

Table 1.

Comparison of the mean profile elevations measured in the field and those obtained from drone flight processing.

Profile # Altitudes	0	5	10	15	20	25	30	35	40	45
H_{GPS}, m	760	759	758	756	754	753	751	749	746	746
H_{UAV},m	719.9	717.9	716.4	714.6	713.2	712.5	711.5	710.4	709.9	708.9
H_{GPS}-H_{UAV}	40.3	41.1	41.3	41.1	40.7	40.2	39.5	38.2	36.6	37.4
Corrected heights	759.5	757.5	756.0	754.2	752.8	752.1	751.1	750.0	749.5	748.5

Table 1 presents the average elevation values along each geophysical profile, measured by the Garmin-65 GPS device (referenced to a geoid-based coordinate system), alongside the corresponding elevation values obtained from UAV-derived data. Differences between datasets are also listed. In particular, a difference of about 3 meters is found between the elevation range measured with a drone (approximately 11 meters) and that measured using field GPS (a range of 14 meters).

This variation implies that, during data interpretation, the relative positioning of anomalous zones may be offset by up to 3 meters. Considering the total dam height of 20 meters, such an error is non-negligible and could significantly influence the accuracy of subsurface anomaly mapping.

A constant correction factor was added to the elevation data derived from the UAV to visualize these discrepancies and align them with the GPS-based measurements. Figure 3 illustrates elevation profiles along the selected measurement lines, showcasing both the field-measured and UAV-derived elevation data. The comparison shows that GPS-based elevation measurements typically vary by ±3 meters, with discrepancies of up to 5-8 meters observed at the ends of profiles, demonstrating the limitations of GPS positioning for high-resolution geophysical surveys. The degree of uncertainty is considerable in the context of a 20-m-high dam, highlighting the requirement for more accurate topographic referencing in similar studies.
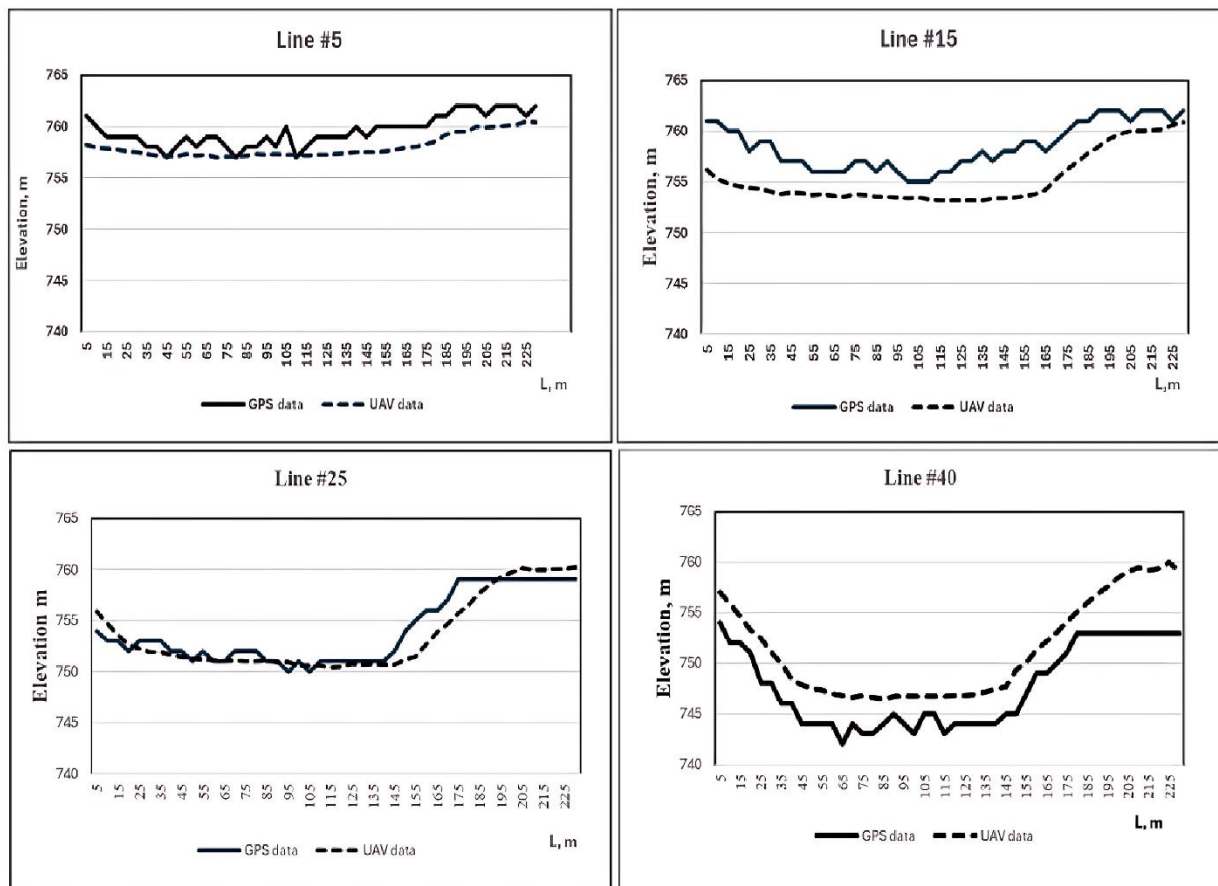
Figure 3.
Comparison of picket elevations from field measurements and those adjusted using drone data for profiles #5, #15, #25, and #45.

4. Results and Discussion

4.1. Resistivity Ranges and Interpretation

A total of ten geophysical profiles were acquired in the field, and the resulting data were processed to construct resistivity distribution sections. The measured resistivity values ranged from 1.3 to 200 Ohm·m. For qualitative interpretation, resistivity values in the range of 1.5 to 20 Ohm·m are associated with highly water-saturated soils, while values above 30 Ohm·m are indicative of naturally moist soils. Intermediate values, between 20 and 30 Ohm·m, suggest partially saturated materials.

Variations in electrical resistivity mainly reflect differences in moisture content and/or lithological composition, including materials such as clays, loams, sandy loams, and sands. In addition, the possible influence of anthropogenic factors such as nearby power lines, pipelines, or reinforced concrete elements should be considered when interpreting anomalous zones, such as nearby power lines, pipelines, or reinforced concrete elements.

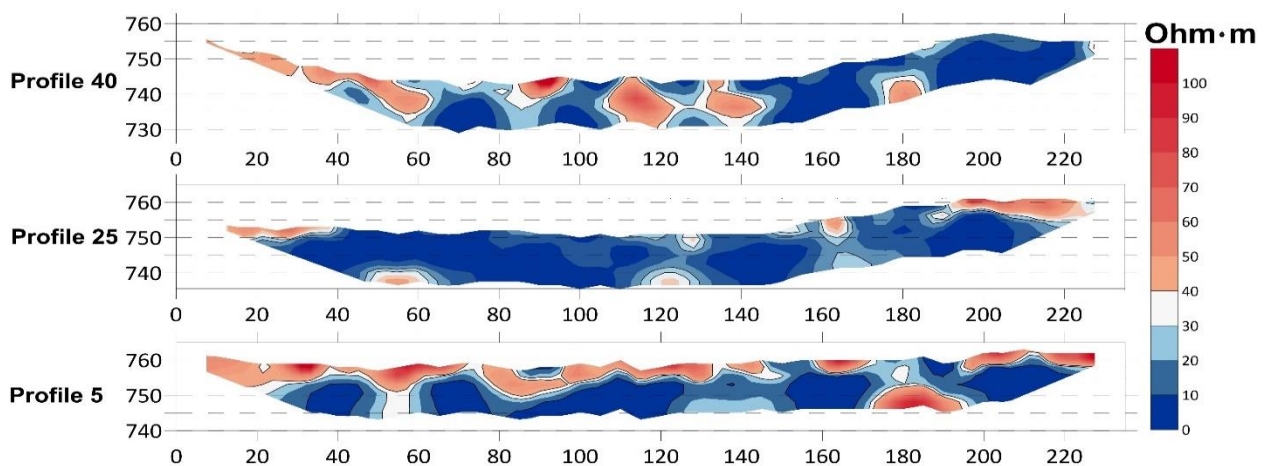Representative geoelectrical sections for profiles #5, #25, and #40 are shown in Figure 4.

Figure 4.
Resistivity section along profiles #5, #25, and #40.

Profile #5:

The electrical resistivity values along this profile range from 7 to 500 Ohm·m. Three distinct low-resistivity zones (<20 Ohm·m), indicating water-saturated soils, are identified at the following intervals:

- 30–45 meters
- 60–120 meters
- 150–170 meters

The first two zones correspond to absolute elevations between 747 and 757 meters. A pronounced seepage zone is already evident in the central part of this section and continues in subsequent profiles.

Profile #25:

The resistivity values range from 7 to 290 Ohm·m. This profile reveals one large and three smaller low-resistivity zones, located at:

- 20–110 meters
- 130–160 meters
- 170–190 meters
- 185–210 meters

These zones occur at absolute elevations ranging from 737 to 757 meters.

Profile #40:

Resistivity values range from 4.5 to 330 Ohm·m. The low-resistivity zone observed in profiles #5 and #25 persists in this profile. Four distinct segments are identified:

- 60–80 meters at 730–745 meters elevation
- 120–130 meters at 727–735 meters
- 145–165 meters at 737–750 meters
- 190–210 meters at 745–747 meters

All geoelectric sections show a heterogeneous internal structure. Water-saturated layers, which vary in thickness, are consistently characterized by apparent resistivity values below 30 Ohm·m. At depths of approximately 15–20 meters, a significant increase in resistivity is observed, reaching 100 Ohm·m or higher, with peak values reaching 700 Ohm·m in certain zones.

Notably, in all analyzed profiles, the thickness of the low-resistivity zone is greater on the left (upstream) side than on the right. This asymmetry suggests that seepage processes from the reservoir are more pronounced near the left-bank abutment of the dam.

4.2. Integration of UAV-DEM into the Interpretation Process

To incorporate elevation data derived from the UAV into the interpretation process, the following correction procedure was implemented:

1. Elevation values for each survey point (picket) were determined using both the Garmin-65 GPS device and UAV data.
2. A constant correction factor of +39.6 meters was added to drone-derived elevations to align them with GPS-based measurements.
3. Interpretations and comparisons were performed using both the corrected UAV data and the original GPS field data.

As a result, drone-based elevation values were assigned to each picket along the profiles. The vertical accuracy of the UAV-derived data was found to significantly exceed that of the GPS measurements obtained in the field.

Although elevation data from the UAV alone would have been sufficient to refine the vertical positions of the electrodes, the horizontal coordinates (longitude and latitude) measured with the Garmin-65 device exhibited noticeable inaccuracy. These positions were not perfectly aligned and deviated from the intended straight-line layout of the survey profiles. Although interpretation software assumes that the electrodes are aligned linearly with uniform spacing, horizontal refinement was still necessary to improve positional accuracy.

Figure 5 illustrates the recorded positions of the electrodes (in red) overlaid on a site map generated in ArcGIS. The measurements were conducted at regular 5-meter intervals. In practice, the electrode cable is laid in a straight line between defined endpoints, meaning that with accurate measurement, the electrode coordinates should also fall in a straight line. However, the figure shows that actual GPS-recorded pickets deviate slightly from this ideal arrangement due to coordinate measurement errors, which affect the uniformity of spacing.

Figure 5.
Layout of profiles and pickets based on field data, constructed using the ArcGIS system.

To correct the horizontal positions of the survey stations within the limits of field measurement accuracy, the following steps were taken:

1. A best-fit regression line was calculated for each profile to approximate the intended straight-line alignment. The equation of the line takes the form:

$$Y = kX + b,$$

where X and Y are the UTM Zone 43N coordinates of the pickets, corresponding to the geographical location of the dam.

2. The midpoint of each profile was identified. The corrected electrode coordinates were then evenly redistributed along the regression line at 5-meter intervals, centered at the original profile midpoint. This ensured that the corrected profile preserved the original center while enforcing uniform spacing and linear alignment.

3. For these refined electrode positions, elevation values were extracted from the UAV-derived digital elevation model (DEM). The elevation correction procedure was subsequently applied to each point.

Figure 6 shows the final adjusted positions of the electrodes (green circles), overlaid on the original GPS points. The corrected points form a straight line with uniform spacing. In most cases, the original and corrected points nearly coincide, indicating only minor adjustments. However, some pickets exhibit visible deviations, likely the result of field GPS errors.
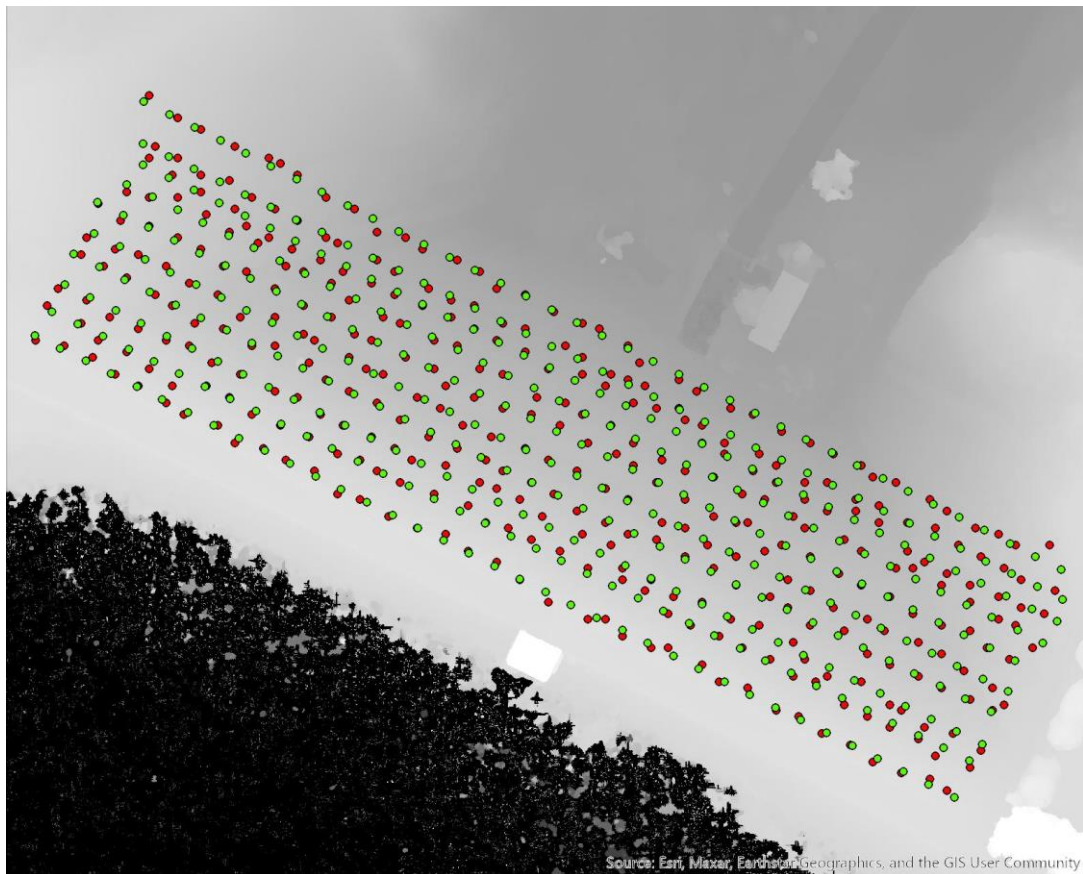
Figure 6.
Layout of the survey electrode positions overlaid on the DSM of the terrain, based on field measurements and drone data.

4.3. Correction of Interpretation Results

Geoelectrical interpretations were carried out using both the original field coordinates of the measurement electrodes and the corrected coordinates derived from UAV-based data integration. A comparison of the resulting resistivity sections is presented in Figures 7, 8, and 9

The analysis revealed that applying elevation corrections produced smoother and more continuous geoelectrical sections, particularly in the vertical direction. These improvements enhance the reliability of subsurface interpretation and demonstrate the positive impact of topographic refinement on inversion results.
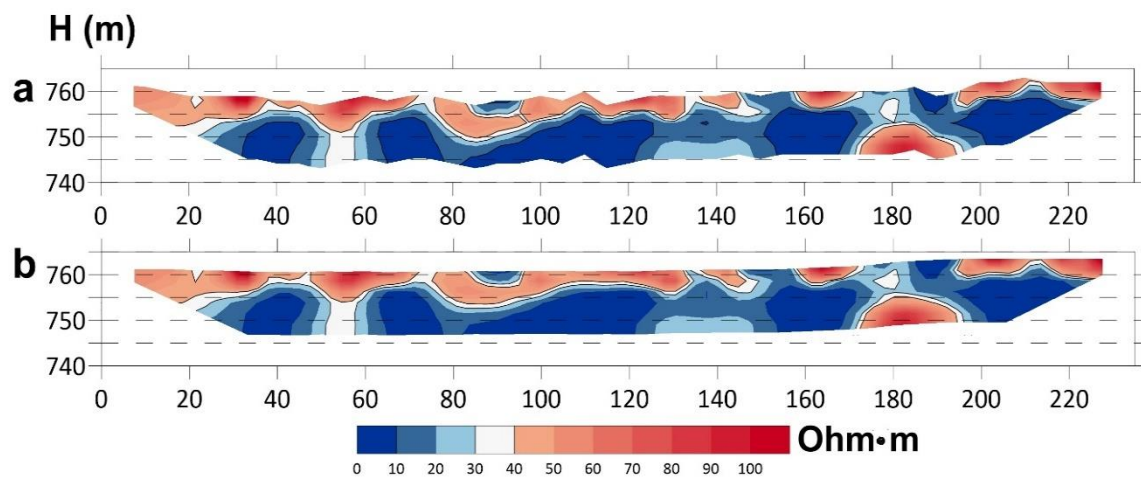

Figure 7.
Electrical resistivity sections along profile #5: (a) original elevation data, (b) corrected elevation data.
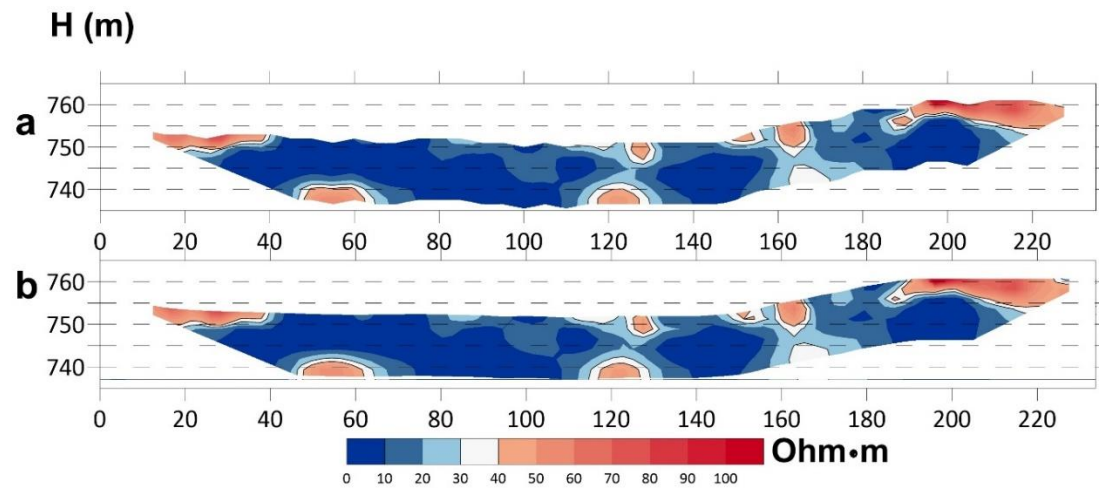
Figure 8.
Electrical resistivity sections along profile #25: (a) original elevation data, (b) corrected elevation data.
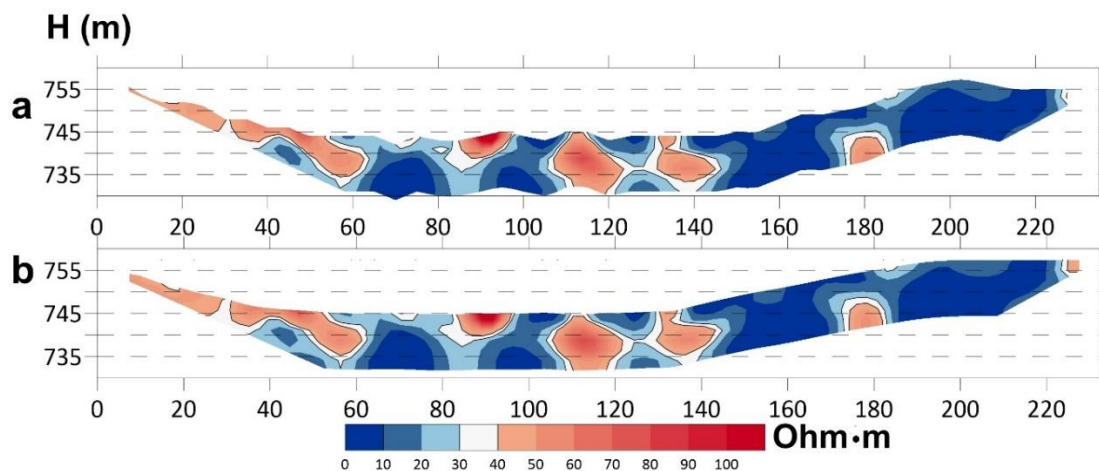

Figure 9.
Electrical resistivity sections along profile #40: (a) original elevation data, (b) corrected elevation data.

We anticipated that correcting the elevation data would lead to significant alterations in the shapes of the geoelectrical sections, thereby affecting the final interpretation outcomes by modifying the geometry of the anomalous zones (Figures 7–9); however, no substantial changes were observed when compared to the initial interpretations. This stability can be attributed to the regularization and smoothing algorithms embedded in the inversion software.[30] which effectively suppresses non-physical oscillations in the resistivity models.

The most noticeable improvement is the smoother representation of the ground surface, particularly evident in profile #5 (Figure 7). Additional, though moderate, changes were observed in profiles #25–45. In profile #25, adjustments are visible in the first and second segments as illustrated in Figure 8. Similarly, profile #40 displays localized modifications, as shown in Figure 9. Despite the absence of drastic structural shifts, the corrected profiles exhibit smoother transitions between zones of contrasting conductivity, which suggests improved accuracy in the delineation of subsurface features. Furthermore, the dam surface in the corrected models appears significantly more regular compared to the original interpretation results.

Similar to the initial interpretation, four low-resistivity zones (with values below 20 Ohm·m) were identified across the profiles, primarily within the 40-200 meter interval (Figure 10). These low-resistivity areas are traceable from one profile to another, suggesting the presence and gradual development of filtration processes within the dam body and its foundation. The zones are typically located at depths of 5 to 15 meters and demonstrate a progressive lateral expansion, indicating possible increases in seepage over time.

The effects of water infiltration, potentially exacerbated by seasonal water level fluctuations, appear to cause surface seepage in the western section of the dam. This is consistent with visual observations of erosion and surface deterioration in that area.

Summary of Interpretation Results is as follows:
- Apparent resistivity values across all profiles range from 4 to 500 Ohm·m;
- All sections contain zones of low resistivity (<20 Ohm·m) indicative of seepage;
- The spatial distribution of these zones shows structural continuity between profiles;
- With each successive profile, filtration zones expand within a depth range of 5 to 20 meters, suggesting gradual water migration through the dam body;

- Four major filtration zones are consistently observed across the profiles, with Zones 2 and 3 merging beneath Profile #5, supporting the conclusion that seepage may reach depths of 15–25 meters;
- Field observations confirm seepage indicators, including the formation of a dry streambed (visible during summer and autumn) on the western slope, and the appearance of a wetland area at the downstream toe of the dam, both likely linked to ongoing filtration.
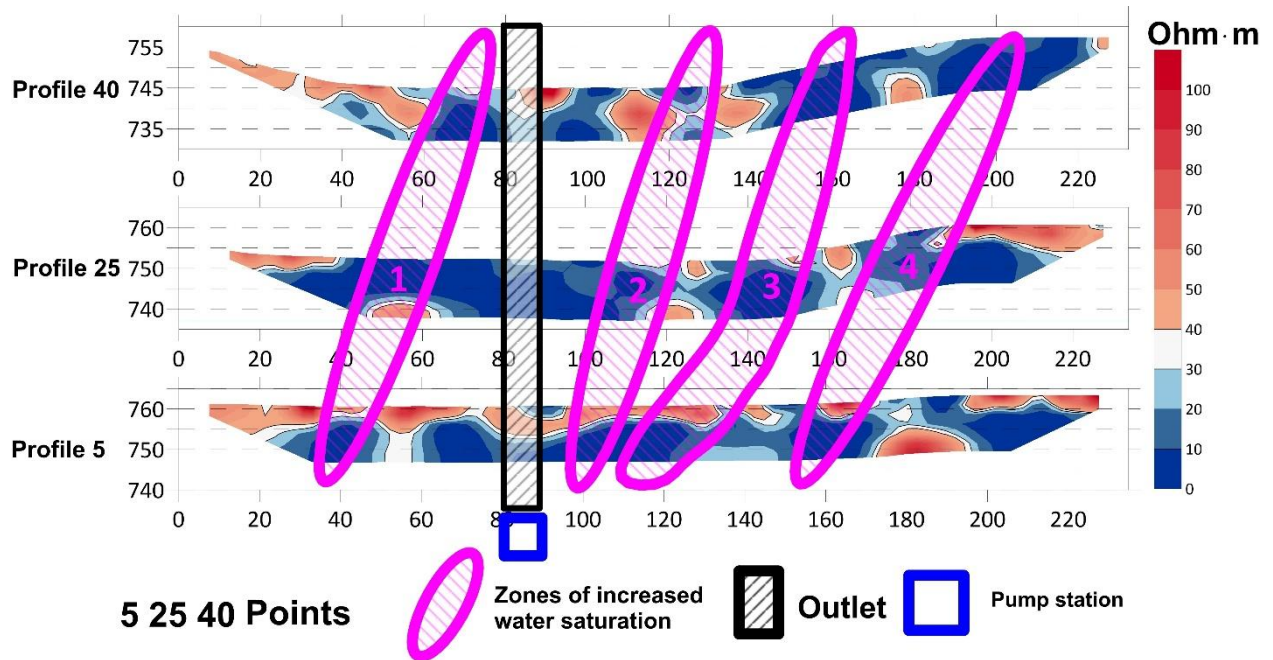

Figure 10.
Geoelectrical sections along profiles #5, 25, and 40 across the K-28 reservoir dam with results of qualitative interpretation.

The absolute error of ERT-derived resistivity models depends on multiple factors, including electrode configuration, inversion regularization, subsurface heterogeneity, and noise. Although the SKALA-48K12 system used here does not specify a fixed percentage error, published field investigations show typical uncertainties in the order of 5–10%, with model deviations less than 8% in comparable environmental applications [37]. The results presented here are supported by visual evidence of seepage. However, to further constrain the nature of the identified anomalies, the use of complementary geophysical techniques such as seismic refraction and ground-penetrating radar is recommended. Coupling geophysical surveys with geotechnical investigations would further strengthen the reliability of diagnostic conclusions.

5. Conclusion

This study demonstrates that when electrode positions in electrical resistivity surveys lack precise geolocation, integrating high-resolution UAV imagery with GIS workflows enables spatial correction and improves geophysical interpretation. The incorporation of UAV-derived digital elevation models (DEMs) into GIS enhances the resolution and reliability of Electrical Resistivity Tomography (ERT), facilitating the detection of subsurface anomalies such as elevated moisture zones and potential seepage pathways. By synthesizing datasets from multiple campaigns and research teams, the approach supports the development of consistent, high-quality dam assessment frameworks.

5.1. Implications

The coordinate correction method proposed in this study improves the spatial accuracy of ERT data, enhancing both real-time monitoring and retrospective analysis of dam conditions. By enabling the reuse of legacy geophysical datasets with corrected electrode positioning, this approach increases the long-term value of previously acquired data and contributes to the development of more consistent and reliable resistivity models. ERT, which combines profiling and vertical sounding, along with its capacity for high-density measurements, supports rapid, non-invasive identification of internal anomalies.

This cost-effective and scalable methodology is particularly relevant for countries like Kazakhstan, where many earthen dams constructed in the 1960s and 1970s have not undergone comprehensive inspection or rehabilitation. In such contexts, ERT offers a practical solution for preliminary large-scale assessments and focused diagnostic surveys. The implementation of systematic UAV-ERT workflows can enable infrastructure managers to detect early signs of structural degradation and plan timely, preventive maintenance. More broadly, this integrated approach provides a transferable framework applicable to similar hydraulic structures in other regions facing aging infrastructure and limited monitoring capacity.

5.2. Limitations

Despite its advantages, the method has several limitations. ERT inversion quality remains sensitive to terrain complexity, subsurface heterogeneity, and high-conductivity surface layers (e.g., clays), which can obscure deeper anomalies. While UAV-based DEMs aid in topographic correction, conventional 2D inversion algorithms may still struggle in steep or complex terrains. Environmental and regulatory constraints, such as weather and UAV flight restrictions, can limit data collection. Additionally, seasonal variations in soil moisture and groundwater levels may introduce inconsistencies in multi-temporal resistivity comparisons. Lastly, effective implementation requires expertise in UAV operation, GIS, and ERT analysis, which may limit adoption in under-resourced regions.

5.3. Future Research

Further integration of ERT and UAV data could be significantly enhanced through the application of mathematical modeling. For instance, Figure 3 illustrates noticeable subsidence in the central section of the dam, indicating deformation relative to its original geometry. Previous studies, Turarova et al. [38] and Mukanova et al. [39], examined the impact of topography on inversion results, evaluating the amplitude of artifacts introduced by surface relief through simplified subsurface models. A method to remove such artifacts was proposed in Turarova et al. [40], but these studies relied on idealized two-dimensional terrain geometries. With UAV technologies, it is now possible to reconstruct real surface geometry and conduct realistic mathematical modeling to assess topographic effects on resistivity measurements and inversion accuracy. This advancement opens new opportunities for terrain-aware corrections and more accurate interpretation.

The authors also intend to extend this research by incorporating both electrical and seismic methods for long-term monitoring of structural changes in hydraulic structures and adjacent areas.

References

[1]   International Commission on Large Dams (ICOLD), "World register of dams: General synthesis," 2024. https://www.icold-cigb.org/GB/world_register/general_synthesis.asp

[2]   A. Moreno-Rodenas, J. D. Mantilla-Jones, and D. Valero, "Age, climate and economic disparities drive the current state of global dam safety," *Nature Water,* vol. 3, no. 3, pp. 284-295, 2025. https://doi.org/10.1038/s44221-025-00402-1

[3]   W. Daily, A. Ramirez, A. Binley, and D. LaBrecque, "Electrical resistance tomography – theory and practice," *The Leading Edge,* vol. 19, no. 6, pp. 642–647, 2000.

[4]   M. J. B. Alam, A. Ahmed, and M. Z. Alam, "Application of electrical resistivity tomography in geotechnical and geoenvironmental engineering aspect," *Geotechnics,* vol. 4, no. 2, pp. 399-414, 2024. https://doi.org/10.3390/geotechnics4020022

[5]   T. Herring *et al.*, "Best practices for using electrical resistivity tomography to investigate permafrost," *Permafrost and Periglacial Processes,* vol. 34, no. 4, pp. 494-512, 2023. https://doi.org/10.1002/ppp.2207

[6]   P. L. Camarero and C. A. Moreira, "Geophysical investigation of earth dam using the electrical tomography resistivity technique," *REM-International Engineering Journal,* vol. 70, no. 1, pp. 47-52, 2017. https://doi.org/10.1590/0370-44672016700099

[7]   W. Al-Fares, "Application of electrical resistivity tomography technique for characterizing leakage problem in Abu Baara earth dam, Syria," *International Journal of Geophysics,* vol. 2014, no. 1, p. 368128, 2014.

[8]   O. Sanuade and A. Ismail, "Geophysical and geochemical pilot study to characterize the dam foundation rock and source of seepage in part of Pensacola Dam in Oklahoma," *Water,* vol. 15, no. 23, p. 4036, 2023. https://doi.org/10.3390/w15234036

[9]   K. Assemov, A. Abetov, and Y. Akhmetov, "Assessment of physical condition and identification of inhomogeneities of the K-25 Earth Dam according to the self-potential method," *International Review of Civil Engineering,* vol. 15, no. 4, 2024. https://doi.org/10.15866/irece.v15i4.24824

[10]   M. Gautier, S. Gautier, and R. Cattin, "PyMERRY: A Python solution for an improved interpretation of electrical resistivity tomography images," *Geophysics,* vol. 89, no. 1, pp. F23-F39, 2024.

[11]   J. Gance, P. Sailhac, and J.-P. Malet, "Corrections of surface fissure effect on apparent resistivity measurements," *Geophysical Journal International,* vol. 200, no. 2, pp. 1118-1135, 2014. https://doi.org/10.1093/gji/ggu453

[12]   Y.-J. Shang *et al.*, "Application of integrated geophysical methods for site suitability of research infrastructures (RIs) in China," *Applied Sciences,* vol. 11, no. 18, p. 8666, 2021. https://doi.org/10.3390/app11188666

[13]   I. Isaev, I. Obornev, E. Obornev, E. Rodionov, M. Shimelevich, and S. Dolenko, "Integration of geophysical methods for solving inverse problems of exploration geophysics using artificial neural networks," in *Problems of Geocosmos–2020: Proceedings of the XIII International Conference and School*, 2022: Springer, pp. 77-87.

[14]   P. Sentenac, V. Benes, and H. Keenan, "Reservoir assessment using non-invasive geophysical techniques," *Environmental Earth Sciences,* vol. 77, no. 7, p. 293, 2018. https://doi.org/10.1007/s12665-018-7463-x

[15]   A. Gabàs, A. Macau, B. Benjumea, F. Bellmunt, S. Figueras, and M. Vilà, "Combination of geophysical methods to support urban geological mapping," *Surveys in Geophysics,* vol. 35, no. 4, pp. 983-1002, 2014. https://doi.org/10.1007/s10712-013-9248-9

[16]   L. Azevedo and A. Soares, *Integration of geophysical data for reservoir modeling and characterization. In Geostatistical Methods for Reservoir Geophysics*. Cham: Springer, 2017.

[17]   H. Zhao *et al.*, "Intelligent segmentation and change detection of dams based on UAV remote sensing images," *Remote Sensing,* vol. 15, no. 23, p. 5526, 2023. https://doi.org/10.3390/rs15235526

[18]   H. Dong, N. Wang, D. Fu, F. Wei, G. Liu, and B. Liu, "Precision and efficiency in dam crack inspection: A lightweight object detection method based on joint distillation for unmanned aerial vehicles (UAVs)," *Drones,* vol. 8, no. 11, p. 692, 2024. https://doi.org/10.3390/drones8110692

[19]   M. Junaid *et al.*, "Discontinuity characterization for slope stability assessment using combined aerial photogrammetry, and geophysics approach," *Natural Hazards,* vol. 121, no. 3, pp. 3581-3600, 2025. https://doi.org/10.1007/s11069-024-06932-3

[20]   Z. Hussain *et al.*, "Mapping, modeling and designing a marble quarry using integrated electric resistivity tomography and unmanned aerial vehicles: A study of adaptive decision-making," *Drones,* vol. 9, no. 4, p. 266, 2025. https://www.mdpi.com/2504-446X/9/4/266

[21]   D. Zumr, V. David, J. Jeřábek, N. Noreika, and J. Krása, "Monitoring of the soil moisture regime of an earth-filled dam by means of electrical resistance tomography, close range photogrammetry, and thermal imaging," *Environmental Earth Sciences,* vol. 79, no. 12, p. 299, 2020. https://doi.org/10.1007/s12665-020-09052-w

[22]   R. Antoine *et al.*, "Geophysical and uav-based observations over a flood defense structure: Application to the Polder2c's experimental dike," *Int. Arch. Photogramm. Remote Sens. Spatial Inf. Sci.,* vol. XLIII-B3-2021, pp. 237-242, 2021. https://doi.org/10.5194/isprs-archives-XLIII-B3-2021-237-2021

[23]   C. Tepeshkin, S. Davydenko, Y. Davydenko, A. Davydenko, A. Parshin, and S. Snopkov, "UAVs and ground-based geophysical surveys and 3D inversion when studying archeological objects in Baykal region," presented at the NSG2021 27th European Meeting of Environmental and Engineering Geophysics, Bordeaux, France, 2021.

[24]   R. Klanica, H. Grison, J. Šteffl, and R. Beránek, "Assessing the volume of defensive structures for architectural energetics analysis using 3D electrical resistivity tomography," *Remote Sensing,* vol. 14, no. 11, p. 2652, 2022. https://doi.org/10.3390/rs14112652

[25]   F. Dadrass Javan, F. Samadzadegan, A. Toosi, and M. van der Meijde, "Unmanned aerial geophysical remote sensing: A systematic review," *Remote Sensing,* vol. 17, no. 1, p. 110, 2025. https://doi.org/10.3390/rs17010110

[26]   S. Zhao, F. Kang, L. He, J. Li, Y. Si, and Y. Xu, "Intelligent structural health monitoring and noncontact measurement method of small reservoir dams using UAV photogrammetry and anomaly detection," *Applied Sciences,* vol. 14, no. 20, p. 9156, 2024. https://doi.org/10.3390/app14209156

[27]   B. Mukanova, T. Mirgalikyzy, K. Tanyrbergenova, K. Assemov, and Y. Akhmetov, "Building of geographic information system for monitoring of dams in the Republic of Kazakhstan," in *Proceedings of the 2024 International Conference on Information Science and Communication Technology (ICISCT) (pp. 145–150). Seoul, Korea*, 2024.

[28]   Garmin, "GPSMAP® 65/65S owner's manual," 2025. https://www8.garmin.com/manuals/webhelp/GUID-EA40F185-39D1-4C3B-B512-7AA823FA3DB5/EN-US/GPSMAP_65_65s_OM_EN-US.pdf. [Accessed Apr. 14, 2025]

[29]   M. Loke, "RES3DMODx64 ver. 3.04: 3-D resistivity and IP forward modeling using the finite-difference and finite-element methods," *Geotomosoft Solutions,* 2014.

[30]   ZondRes2d [Computer Software], "Zond geophysical software," 2025. http://zond-geo.com/english/zond-software/ert-and-ves/zondres2d/. [Accessed Jan. 15, 2025]

[31]   M. E. Everett, *Near-surface applied geophysics*. Cambridge, UK: Cambridge University Press, 2013.

[32]   SKALA-46k12, "Operator instruction manual, KB Electrometry, Russia," 2025. https://kbelectrometry.ru/wp-content/uploads/2021/04/SibER-48K12-64K15-operator-instruction_rus.pdf. [Accessed Mar. 15, 2025]

[33]   DJI, "Phantom 4 RTK specifications," 2025. https://ag.dji.com/phantom-4-rtk/specs. [Accessed Jan. 15, 2025]

[34]   DJI, "DJI Terra user manual," 2024. https://www.dji.com/global. [Accessed Jan. 15, 2025]

[35]   Esri, "ArcGIS pro overview," 2025. https://www.esri.com/en-us/arcgis/products/arcgis-pro/overview. [Accessed Jan. 15, 2025]

[36]   NOAA/National Geodetic Survey, "GeoidEval – online geoid height calculation tool," 2022. https://geodesy.noaa.gov/

[37]   K. Basri, N. Wahab, M. K. A. Talib, and A. Zainorabidin, "Sub-surface profiling using electrical resistivity tomography (ERT) with complement from peat sampler," *Civil Engineering and Architecture,* vol. 7, no. 6A, pp. 7-18, 2019.

[38]   M. K. Turarova, T. Mirgalikyzy, B. G. Mukanova, I. N. Modin, and P. A. Kaznacheev, "Evaluation of the 3D topographic effect of homogeneous and inhomogeneous media on the results of 2D inversion of electrical resistivity tomography data," *Modelling and Simulation in Engineering,* vol. 2022, no. 1, p. 5196686, 2022. https://doi.org/10.1155/2022/5196686

[39]   B. Mukanova, M. Turarova, and D. Rakisheva, "Longitudinal electrical resistivity tomography interpretation: Numerical modelling," *Geophysical Prospecting,* vol. 73, no. 2, pp. 680-698, 2025. https://doi.org/10.1111/1365-2478.13614

[40]   M. Turarova, T. Mirgalikyzy, B. Mukanova, and I. Modin, "Elimination of the ground surface topographic effect in the 2D inversion results of electrical resistivity tomography data," *Eurasian Journal of Mathematical and Computer Applications,* vol. 10, no. 3, pp. 84-104, 2022.